Polymer defect states modulate open-circuit voltage in bulk-heterojunction solar cells

Teresa S. Ripolles, Antonio Guerrero, and Germà Garcia-Belmonte

Citation: Appl. Phys. Lett. **103**, 243306 (2013); doi: 10.1063/1.4841475
View online: http://dx.doi.org/10.1063/1.4841475
View Table of Contents: http://apl.aip.org/resource/1/APPLAB/v103/i24
Published by the AIP Publishing LLC.

Polymer defect states modulate open-circuit voltage in bulk-heterojunction solar cells

Teresa S. Ripolles, Antonio Guerrero, and Germà Garcia-Belmonte[a)]
Photovoltaic and Optoelectronic Devices Group, Departament de Física, Universitat Jaume I, ES-12071 Castelló, Spain

(Received 7 October 2013; accepted 18 November 2013; published online 13 December 2013)

Defect states influence the operation of organic solar cells altering transport, recombination, and energetic mechanisms. This work investigates how processing conditions induce morphology-related, electrically active defects in the donor polymer of bulk-heterojunction solar cells. Structural order is inferred from absorption and X-ray diffraction data, while defect density is determined from capacitance methods. A correlation is observed between the polymer nanocrystallite size, the defect concentration, and the output voltage. For the case of poly(3-hexylthiophene), processing that promote crystallinity is beneficial for the device performance as it decreases the defect density (energy disorder) that finally enlarges the maximum achievable open-circuit voltage. Defect states within the effective bandgap modulate the downshift of the hole Fermi level upon illumination that in turn establishes the achievable open-circuit voltage. © *2013 AIP Publishing LLC*. [http://dx.doi.org/10.1063/1.4841475]

Organic photovoltaic (OPV) devices have recently witnessed an impressive improvement in the power conversion efficiency (PCE) now reaching 9.2%.[1] In a bulk heterojunction device, a conjugated polymer donor is intimately blended with a fullerene acceptor molecule. In this configuration, materials form a highly connected, interpenetrating network, in which generation of excitons give rise to separated charges at the donor-acceptor interface enabling an efficient transport of carriers towards the electrodes.[2] The nanoscale morphology can be controlled by a number of ways such as the selection of appropriate solvents,[3,4] drying processes,[5] donor:acceptor ratio,[4] concentration of materials,[6] thermal treatments,[2,7] or use of additives.[8] Processing conditions of the films control the blend morphology which is then critical to ultimately improve the photovoltaic parameters and OPV performance.[4,9]

One of the strategies to enlarge the open-circuit voltage V_{oc} consists on reducing charge recombination flux.[10] Limiting recombination pathways increases the amount of free carriers within the active layer in operating conditions which in turn modifies the Fermi level position of electrons (E_{Fn}) and holes (E_{Fp}), and ultimately the output voltage as[11]

$$qV_{oc} = E_{Fn} - E_{Fp}. \quad (1)$$

Another factor influencing photovoltage has a purely energetic origin. Energy disorder of both fullerene acceptor and polymer donor induces bandgap density-of-states (DOS) (exponential or Gaussian tails and traps) that modulate the light-induced Fermi level shift.[12] This last mechanism explains how processing conditions, which modify the structural order and crystallinity of the active layer compounds, can alter the output V_{oc}. Recent studies have found that variations within the fullerene DOS related to their dissimilar aggregation ability affect the final achieved V_{oc}.[13] It was observed that large fullerene DOS limits the Fermi level upward shift yielding as a result lower V_{oc} values. However, the influence on photovoltage of the polymer energetic disorder/crystallinity has been much less explored.[14] How processing conditions induce morphology-related electronic defects in the donor polymer and the repercussion on the achieved V_{oc} will be the specific aim of this work.

One of the most commonly studied OPV system is based in the semicrystalline blend composed by the donor material poly(3-hexylthiophene) (P3HT) and the acceptor fullerene derivate [6,6]-phenyl-C61-butyric acid methyl ester ($PC_{60}BM$) with reported efficiencies around 3%-5%.[15] The efficiency of P3HT:$PC_{60}BM$ solar cells are drastically improved upon annealing as the P3HT-crystallinity is increased leading to improved optical absorption and transport of carriers.[3] The fibrillar-like P3HT crystals are embedded in a matrix mainly comprised by $PC_{60}BM$ nanocrystals and amorphous P3HT.[16] As it will be shown here, a clear correlation between the crystallinity of materials and the concentration of electrically active defects is observed. Moreover, we show how polymer structural order and defect density modulate the achievable output voltage.

The studied polymer photovoltaic devices are fabricated in the configuration glass/ITO/P3HT:$PC_{60}BM$/Ca/Ag.[17] PEDOT:PSS was deposited by spin coating over clean ITO to provide a film thickness of about 35 nm. Films were dried followed by deposition of the active layer P3HT:$PC_{60}BM$. Some samples were slowly dried, spin coating was carried out at 900 rpm for 10 s, and then substrates were introduced into a petri dish and covered for 2 h (devices 1 and 2). Other samples were completely dried during the spin coating process at 3500 rpm for 2 min. These are denoted as fast drying devices. Films were heated at the temperatures stated in Table I. The active layer thickness of the film was approximately 300 nm. Finally, the cathode electrode was deposited (5 nm Ca/100 nm Ag) by thermal evaporation for all samples at a base pressure below 3×10^{-6} mbar. The devices were then encapsulated with epoxy and a glass slide before

[a)]Author to whom correspondence should be addressed. Electronic mail: garciag@uji.es. Tel.: +34 964 387538. Fax: +34 964 729218

TABLE I. Photovoltaic parameters of P3HT:$PC_{60}BM$ measured under 1 sun illumination using different processing conditions. Defect density n extracted from capacitance-voltage measurements under dark conditions and at 100 Hz. P3HT domain size L calculated from XRD data.

Device	Conditions	j_{sc} (mA cm^{-2})	V_{oc} (mV)	*FF* (%)	*PCE* (%)	n ($\times 10^{16}$) (cm^{-3})	L (nm)
1	Slow dry	7.31	566	54	2.2	4.0	14
2	Slow dry, 130 °C[a]	7.57	621	64	3.0	0.2	21
3	Fast dry	2.45	587	32	0.5	1.2	14
4	Fast dry, 90 °C	7.67	572	54	2.4	2.0	18
5	Fast dry, 130 °C	8.28	608	50	2.6	0.4	18

[a]Post-cathode annealing.

testing. An additional thermal treatment at 130 °C for 10 min was carried out for device 2 noted as post-cathode annealing. More experimental details can be found as supplementary material.[29]

Active layer morphology is varied by either a control of the drying time of the film (long drying times for device 1), by a thermal treatment of the deposited films (devices 3–5), or by both conditions (device 2). Absorption spectra of the films are shown in Fig. 1(a). The absorption spectrum of a neat film containing P3HT has been added as a reference. Results are similar to previously reported experiments.[3,18] Below 400 nm, the absorption of $PC_{60}BM$ is dominant[19] and the P3HT band is visible between 400 and 650 nm. At about 500 nm, it is observed a characteristic peak that provides information on the degree of conjugation of the P3HT chains, and a peak at around 600 nm informs on the degree of interchain order.[5,20] Figure 1(a) shows red-shifted absorbance of the slow dried P3HT:$PC_{60}BM$ films (device 1),

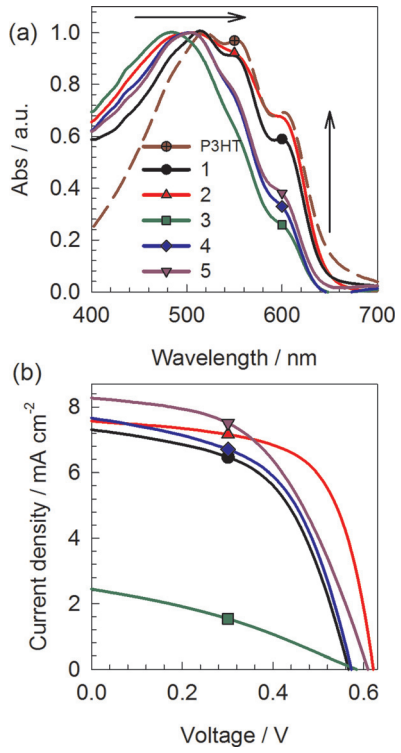

FIG. 1. (a) UV-Vis absorbance spectra of films deposited from P3HT:$PC_{60}BM$ blends. The spectra have been normalized to the maximum of the P3HT peak at around 500 nm. Devices correspond to those listed in Table I. (b) Current density vs. applied voltage plot measured under simulated 1 sun illumination for the devices fabricated in this work.

indicating longer polymer conjugation lengths than the fast dried samples (devices 3–5) and a narrower bandgap. In fact, the band gap decreases about 85 meV, when comparing the less crystalline sample (device 3) with the more crystalline film (device 2). The height of the vibronic shoulder at 600 nm increases systematically from fast drying and un-annealed film (device 3) to fast drying, 130 °C-annealed film (device 5), being even higher for P3HT:$PC_{60}BM$ slow drying films (devices 1 and 2). These results indicate a poor degree of interchain order for the un-annealed P3HT:$PC_{60}BM$ film. The P3HT-polymer film absorbance spectra exhibit a slightly larger absorbance at 600 nm respect to the other blend films which evidences that the introduction of fullerene as $PC_{60}BM$ into the blend film disturbs the polymer local ordering. These experiments show that absorption measurements are very sensitive to differences in crystallinity. In addition, XRD data of our films (see supplementary material) exhibit a diffraction peak that correspond to the *a*-axis orientation related to the packing of the alkyl chains of the P3HT crystallites. From the width and position of the diffraction peak, an estimation of the P3HT nanodomain size is calculated (see supplementary material), which results within the range of 15–20 nm (Table I). Unfortunately, XRD data do not provide any information on the *b*- or *c*-axis orientations and consequently valuable information on the packing of the thiophene rings is missing. Crystallinity issues will be discussed relying upon variations in absorption features, particularly the relative height of the vibronic shoulder at 600 nm with respect to the maximum at ~500 nm and crystallite size extracted from XRD data.

The photovoltaic parameters of P3HT:$PC_{60}BM$ devices are summarized in Table I and current density-voltage $j-V$ curves measured under AM1.5G illumination (1000 W m^{-2}) are shown in Fig. 1(b). Similar results are obtained for deposition conditions in which crystallinity has been enhanced either by controlling the drying process or through a thermal treatment. Only the least crystalline film dried fast with no annealing treatment (device 3) shows a remarkably lower short-circuit current (j_{sc}) and fill factor. The $j-V$ curves are in agreement with previously reported results in which film morphology is modified with similar processes.[21] Remarkably, the most crystalline film (device 2) provides higher V_{oc}.

Although absorption spectra in Fig. 1(a) and XRD data reveal variations in the polymer structural order among samples, they do not allow for a direct quantification of electrically active morphological features. For this reason, it is necessary to explore the response to purely electrical

methods. It is believed that larger polymer ordering gives rise to smaller amounts of structural defects originated at less crystalline zones where the periodic spacing is broken. Polymer defect states acting as acceptor impurities might originate free holes, as evidenced by monitoring the polymer conductivity or photoluminescence quenching.[22] The density of defect states is accessible by means of capacitive methods that measure the width of the depletion zone built-up in the vicinity of the cathode contact. Here, we use capacitance-voltage measurements carried out in dark conditions from −1 to 0.5 V at constant frequency of 100 Hz following previously described methods.[23] The Mott-Schottky plots $C^{-2} - V$ are shown in Fig. 2(a), exhibiting a linear relation given by the following expression

$$C^{-2} = \frac{2}{A^2 q \varepsilon \varepsilon_0 n}(V_{fb} - V). \quad (2)$$

Here, A corresponds to the device active surface, ε is the relative dielectric constant of the blend ($\varepsilon \approx 3$), ε_0 is the permittivity of the vacuum, V_{fb} is the flat-band potential, and n is the total concentration of defects (doping level). Then, using Eq. (2), the concentration of electrically active acceptor impurities n and V_{fb} can be extracted at reverse and low forward bias from the slope and the extrapolated intersection with the voltage axis, respectively (Table I). Interestingly, the Mott-Schottky plot does not show full depletion at −1 V for most of the devices, except for the most crystalline film (device 2) in which the geometric capacitance can be derived from the saturation at reverse bias.

It is important to note that devices have not been exposed to air at any time. Then, the measured defect densities should mainly correspond to intrinsic, structural impurities/defects of the active layer rather than originated by air-related polymer oxidation.[24] Recalling now absorption measurements, it is observed that increasing the crystallinity of the polymer leads to decreased doping densities. Indeed, processing conditions that provide poorly crystalline blends such as devices 3 and 4 show relatively higher doping densities. In contrast, for a device annealed after a slow drying process (device 2), the doping density is about one order of magnitude lower than those observed for devices 3 and 4. Then, it appears that the defects are related to the actual surface area of the polymer crystallites. It is plausible to assume that polymer molecules present at the boundary between regular domains will show a different energetic landscape than those molecules found in the middle of a crystallite. Then, the doping density decreases at higher temperatures as the P3HT molecules aggregates enabling for a less disperse energetic landscape. For comparison purposes, devices based on the highly amorphous system PCDTBT:$PC_{70}BM$ have been measured (see the XRD spectra and the Mott-Schottky plot in supplementary material). For this system, doping density of 1.4×10^{17} cm^3 has been observed which is two orders of magnitude higher than those observed for device 2. These results further suggest that the doping density is highly related to the polymer and its degree of structural order.

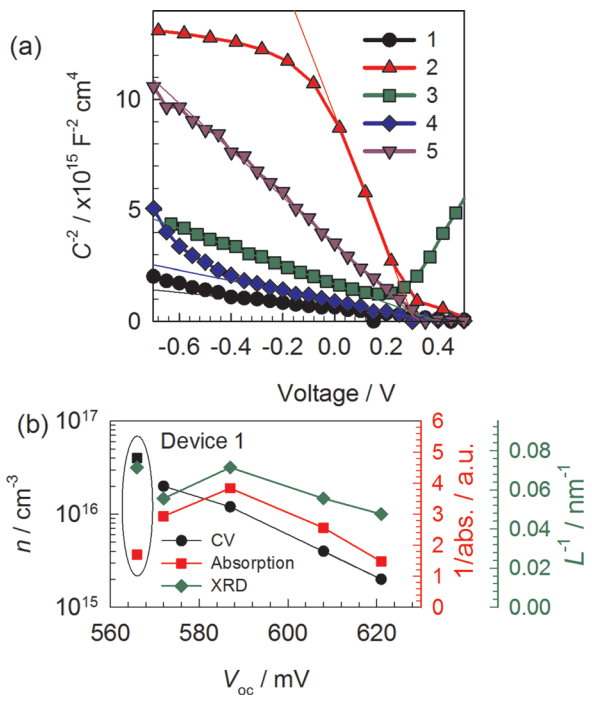

FIG. 2. (a) Mott-Schottky curves in dark conditions from −1 to 0.5 V measured at constant frequency of 100 Hz for P3HT:$PC_{60}BM$ devices listed in Table I. (b) Defect density n extracted from CV analysis, inverse of the relative P3HT absorption intensity peak at 600 nm, and inverse of the crystallite nanodomain size L from XRD data vs. open-circuit voltage. Device 1 parameters do not follow the general trend.

As reported previously, V_{oc} is related to the HOMO level of the Donor and the LUMO level of the acceptor,[25] and more precisely to the difference in Fermi levels of electrons and holes of Eq. (1). It is known that thermal treatment produces an upward shift of the polymer HOMO manifold.[26] This is indeed confirmed by the red-shifted absorption spectra in Fig. 1(a). Therefore, V_{oc} for device 3 should show an increase of about 40 meV (85 meV is the difference in bandgap) in comparison with device 2 caused by differences in the polymer bandgap. However, the observed trend in our experiments is just the opposite as device 3 shows a V_{oc} about 35 mV lower than that observed for device 2. Then it is clear that apart from the effective bandgap of the materials there may be other factors affecting the achievable V_{oc}. We remark here that there exists a correlation between the polymer disorder degree (lack of crystallinity) and the defect density as observed from the doping level extracted by means of capacitive tools.

By examining Fig. 2(b), one can observe an exponential trend between the calculated doping density from capacitance analysis and V_{oc} for the P3HT:$PC_{60}BM$ system, in which V_{oc} increases with a reduction of the impurities. The right axes of Fig. 2(b) correspond to a measurement of the polymer structural order, extracted either from the inverse value of the nanodomain size (XRD data) or from the inverse of the relative P3HT absorption intensity peak of the vibronic shoulder at 600 nm (data extracted from Fig. 1(a)). Inverse values are used here in order to directly compare with density measurements. It is observed that crystallinity degree and defect density correlate with the achieved V_{oc}. It is worth noting that P3HT crystallite size corresponds to a concentration of order of 10^{17} cm^{-3} in good accordance with the defect density encountered ($10^{15} - 10^{16} cm^{-3}$). The trends are observed in Fig. 2(b) for the studied devices with the exception of device 1. This is a special case (slow drying

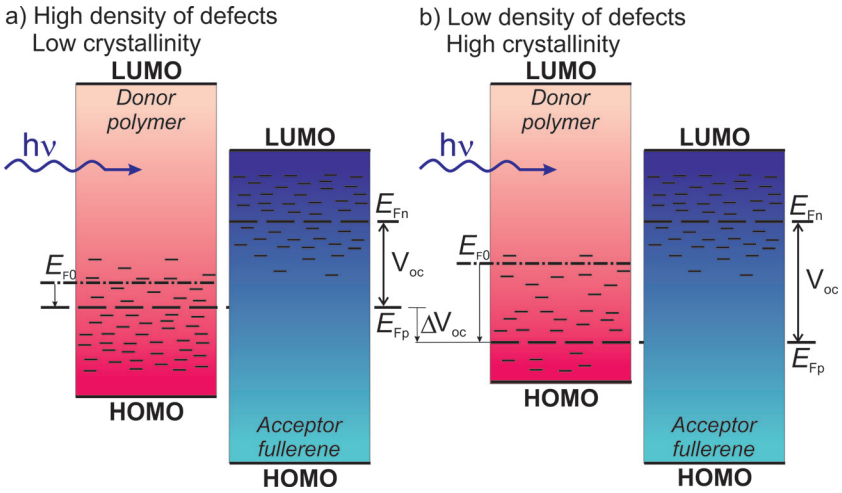

FIG. 3. Energy diagram of the polymer:fullerene blend under illumination indicating the electrically active states in the band gap of both materials. The donor HOMO level is displaced depending on the polymer crystallinity. The position of the equilibrium (dark) Fermi level is signaled as E_{F0}. The splitting of the hole Fermi Level (E_{Fp}) and the electron Fermi Level (E_{Fn}) yields the output open-circuit voltage. Two extreme cases of (a) high and (b) low defect density are shown. Lower-lying levels are occupied in the case of low defect density which produces the open-circuit voltage difference ΔV_{oc}.

without thermal treatment) in which residual solvent might be present as a source of external chemical impurities that contribute to increase the doping density. Then, in spite that slow drying promotes crystallinity, the output V_{oc} exhibited by device 1 is the lowest. This exception would imply that defect density rather than the actual structural order lies behind the achieved V_{oc}.

Only by considering differences in j_{sc} and the diode equation is not possible to explain the observed variations in V_{oc} among solar cells. The electronic effect of gap defects is linked with their ability to modulate the position of the hole Fermi level E_{Fp}, which in fact establishes the achievable V_{oc}. Under illumination conditions, E_{Fp} undergoes a downward shift with respect to the equilibrium Fermi level E_{F0} which is situated at an upper lying level for more crystalline polymers (see Fig. 3). Energy shift results larger when defect density is smaller because there are less available electronic states within the bandgap to be occupied by photogenerated charges. Then more crystalline samples that exhibit lower defect density allow for a larger E_{Fp} downshift. Therefore, the defect effect is dominant over variations in the band gap and it determines the final achievable V_{oc}. For simplicity, we consider in Fig. 3 that the number of defects created from different processing conditions and/or other annealing treatments, affects mainly the polymer. Figures 3(a) and 3(b) represent high and low density of defects of the polymer for a standard photovoltaic device under illumination, respectively. Without the decrease in the bandgap, the maximum achievable V_{oc} should be about 40 mV higher reaching values of about 660 mV. Electronic states corresponding to fullerene molecules might also vary under different device processing[27] or even more when different fullerenes derivatives are used.[28] This alters the position of the electron Fermi level and the final output V_{oc} as discussed in the previous work comparing the influence of the acceptor LUMO level bandgap tails.[13] Here, we highlight the effect of polymer structural order and how it influences (modulates) the light-induced shift of E_{Fp}. In conclusion, we have shown that device processing that enables an increased crystallinity of the film is beneficial for the device performance as it decreases the defect density (energy disorder) that finally enlarges the maximum achievable V_{oc}, despite the upward shift of the polymer HOMO manifold.

We thank financial support from Generalitat Valenciana (Prometeo/2009/058) and ISIC/2012/008 Institute of Nanotechnologies for Clean Energies. SCIC services at UJI are acknowledged.

[1]Z. He, C. Zhong, S. Su, M. Xu, H. Wu, and Y. Cao, Nature Photonics **6**, 591–595 (2012).
[2]X. N. Yang, J. Loos, S. C. Veenstra, W. J. H. Verhees, M. M. Wienk, J. M. Kroon, M. A. J. Michels, and R. A. J. Janssen, Nano Lett. **5**(4), 579 (2005).
[3]U. Zhokhavets, T. Erb, G. Gobsch, M. Al-Ibrahim, and O. Ambacher, Chem. Phys. Lett. **418**(4–6), 347 (2006).
[4]G. Dennler, M. C. Scharber, and C. J. Brabec, Adv. Mater. (Weinheim, Germany) **21**(13), 1323 (2009).
[5]B. F. Xue, B. Vaughan, C. H. Poh, K. B. Burke, L. Thomsen, A. Stapleton, X. J. Zhou, G. W. Bryant, W. Belcher, and P. C. Dastoor, J. Phys. Chem. C **114**(37), 15797 (2010).
[6]S. Wakim, S. Beaupre, N. Blouin, B.-R. Aich, S. Rodman, R. Gaudiana, Y. Tao, and M. Leclerc, J. Mater. Chem. **19**(30), 5351 (2009).
[7]F. Padinger, R. S. Rittberger, and N. S. Sariciftci, Adv. Funct. Mater. **13**(1), 85 (2003).
[8]T. Y. Chu, S. Alem, S. W. Tsang, S. C. Tse, S. Wakim, J. P. Lu, G. Dennler, D. Waller, R. Gaudiana, and Y. Tao, Appl. Phys. Lett. **98**(25), 253301 (2011).
[9]M. A. Brady, G. M. Su, and M. L. Chabinyc, Soft Matter **7**, 11065 (2011).
[10]A. Maurano, R. Hamilton, C. G. Shuttle, A. M. Ballantyne, J. Nelson, B. O'Regan, W. Zhang, I. McCulloch, H. Azimi, M. Morana, C. J. Brabec, and J. R. Durrant, Adv. Mater. **22**, 4987 (2010).
[11]G. Garcia-Belmonte and J. Bisquert, Appl. Phys. Lett. **96**, 113301 (2010); J. Widmer, M. Tietze, K. Leo, and M. Riede, "Open-circuit voltage and effective gap of organic solar cells," Adv. Funct. Mater. (published online).
[12]J. C. Blakesley and D. Neher, Phys. Rev. B **84**, 075210 (2011); J. A. Carr and S. Chaudhary, Energy Environ. Sci. **6**, 3414–3438 (2013).
[13]G. Garcia-Belmonte, P. P. Boix, J. Bisquert, M. Lenes, H. J. Bolink, A. L. Rosa, S. Filippone, and N. Martín, J. Phys. Chem. Lett. **1**, 2566 (2010); A. Sánchez-Díaz, M. Izquierdo, S. Filippone, N. Martin, and E. Palomares, Adv. Funct. Mater. **20**, 2695 (2010).
[14]Z. M. Beiley, E. T. Hoke, R. Noriega, J. Dacuña, G. F. Burkhard, J. A. Bartelt, A. Salleo, M. F. Toney, and M. D. McGehee, Adv. Energy Mater. **1**, 954 (2011).
[15]E. J. Luber and J. M. Buriak, ACS Nano **7**(6), 4708 (2013).
[16]N. D. Treat, M. A. Brady, G. Smith, M. F. Toney, E. J. Kramer, C. J. Hawker, and M. L. Chabinyc, Adv. Energy Mater. **1**(1), 82 (2011); H. W. Ro, B. Akgun, B. T. O'Connor, M. Hammond, R. J. Kline, C. R. Snyder, S. K. Satija, A. L. Ayzner, M. F. Toney, C. L. Soles, and D. M. DeLongchamp, Macromolecules **45**(16), 6587 (2012).
[17]A. Guerrero, T. Ripolles-Sanchis, P. P. Boix, and G. Garcia-Belmonte, Org. Electron. **13**(11), 2326 (2012).
[18]P. Vanlaeke, A. Swinnen, I. Haeldermans, G. Vanhoyland, T. Aernouts, D. Cheyns, C. Deibel, J. D'Haen, P. Heremans, J. Poortmans, and J. V. Manca, Sol. Energy Mater. Sol. Cells **90**(14), 2150 (2006); M. Campoy-Quiles, T. Ferenczi, T. Agostinelli, P. G. Etchegoin, Y. Kim, T. D.

Anthopoulos, P. N. Stavrinou, D. D. C. Bradley, and J. Nelson, Nature Mater. **7**(2), 158 (2008).
[19]R. B. Aich, Y. P. Zou, M. Leclerc, and Y. Tao, Org. Electron. **11**(6), 1053 (2010).
[20]P. J. Brown, D. S. Thomas, A. Kohler, J. S. Wilson, J. S. Kim, C. M. Ramsdale, H. Sirringhaus, and R. H. Friend, Phys. Rev. B **67**(6), 064203 (2003).
[21]W. Ma, C. Yang, X. Gong, K. Lee, and A. J Heeger, Adv. Funct. Mater. **15**(10), 1617 (2005); G. Li, V. Shrotriya, J. Huang, Y. Yao, T. Moriarty, K. Emery, and Y. Yang, Nature Mater. **4**(11), 864 (2005).
[22]Z. Liang and B. A. Gregg, Adv. Mater. **24**, 3258 (2012).
[23]F. Fabregat-Santiago, G. Garcia-Belmonte, I. Mora-Sero, and J. Bisquert, Phys. Chem. Chem. Phys. **13**(20), 9083 (2011).
[24]A. Guerrero, P. P. Boix, L. F. Marchesi, T. Ripolles-Sanchis, E. C. Pereira, and G. Garcia-Belmonte, Sol. Energy Mater. Sol. Cells **100**, 185 (2012); O. V. Kozlov and S. A. Zapunidi, Synth. Met. **169**, 48 (2013).
[25]M. C. Scharber, D. Mühlbacher, M. Koppe, P. Denk, C. Waldauf, A. J. Heeger, and C. J. Brabec, Adv. Mater. (Weinheim, Germany) **18**(6), 789 (2006).
[26]H. Aarnio, P. Sehati, S. Braun, M. Nyman, M. P. de Jong, M. Fahlman, and R. Österbacka, Adv. Energy Mater. **1**, 792 (2011).
[27]E. Verploegen, R. Mondal, C. J. Bettinger, S. Sok, M. F. Toney, and Z. Bao, Adv. Funct. Mater. **20**, 3519 (2010).
[28]K. Akaike, K. Kanai, Y. Ouchi, and K. Seki, Chem. Phys. **415**, 31 (2013).
[29]See supplementary material at http://dx.doi.org/10.1063/1.4841475 for experimental details, XRD data, and Mott-Schottky analysis.